GISAXS View of Vanadium/Cerium Oxide Thin Films and Influence of Lithium Intercalation

M. Lučić Lavčević,*,† P. Dubček,‡ Z. Crnjak Orel,§ and A. Turković‡

Department of Physics, Faculty of Chemical Technology, University of Split, Teslina 10, 21000 Split, Croatia, Institute Ruđer Bošković, P. O. Box 10002, Zagreb, Croatia, and National Institute of Chemistry, Hajdrihova 19, SI-1001 Ljubljana, Slovenia

Received April 26, 2005

An examination of structural modifications, induced by mixing vanadium and cerium oxides and by the introduction of lithium in vanadium and mixed vanadium/cerium oxide films, was performed using synchrotron sourced grazing incidence small-angle X-ray scattering. Samples were sol−gel-derived films, deposited by a dip-coating technique. An analysis of the scattering data, acquired by a two-dimensional detection system, is based on the comparison of the surface and bulk characteristics of the film. The trend of estimated structural modifications is supported by the results of previous investigations on a different length scale, performed by atomic force microscopy.

1. INTRODUCTION

The demands on electrode material, which undergoes lithium intercalation in advanced electrochemical cells and electrochromic devices, are rather stringent. In the first place, such electrodes should maintain their integrity over many discharge−recharge cycles, but they should also have significant capacity for lithium ions and stable electrochemical performances. Not all demands can be satisfied by a single material. Small lithium ions can fit into spaces between atoms in a variety of materials, especially in those with layered structures, but electrode performance has to be enhanced by composing materials. In addition, to exploit the desirable properties of each component and avoid the undesirable ones, disorder on different length scales can be introduced into the electrode structure. This requirement for electrodes designed down to nanosized scale highlights the potential of materials with nanostructural characteristics.

Characterizations of sol−gel-derived films of various metal oxides suggest that they are porous nanostructures with a large inner surface area, which makes them suitable candidates for electrodes in various applications.[1−5] In this paper, we focus on sol−gel-derived films of selected vanadium and cerium oxides. Vanadium pentoxide (V_2O_5) films have a layered structure that is suitable for the intercalation of small ions.[6] As electrodes, they show long-term durability.[7] Cerium dioxide (CeO_2) containing films show very good capacity for lithium intercalation. Their transparency, crucial for applications in electrochromic devices, does not depend on lithium ion content.[8] Previous examinations of film samples, prepared by the sol−gel procedure at different concentrations of V in V_2O_5/CeO_2 (from this point on, V/Ce oxides), showed that mixed oxides exhibit enhanced electrochemical stability.[9] As the best performances were obtained by a sample prepared at 38 atom % of V in V/Ce oxide,[9,10] this sample should have an especially suitable structure for the intercalation of lithium ions. Additionally, an interesting behavior of this particular sample under intercalation of lithium was registered in determining its surface characteristics by atomic force microscopy (AFM).[10] Namely, vanadium oxides exhibit a trend of lowering the surface roughness under lithium intercalation. On the other hand, V/Ce oxide with 38 atom % of V, with an originally smooth surface, exhibits an increase of surface roughness under lithium intercalation. This is well-demonstrated by Figure 1, in which AFM micrographs are presented, recorded for V oxide and V/Ce oxide with 38 atom % of V before and after lithium intercalation.

Following these results, we performed an analysis of structural modifications, induced by mixing vanadium and cerium oxides and by introduction of lithium in vanadium and mixed vanadium/cerium oxide films, using the grazing incidence small-angle X-ray scattering (GISAXS) technique. The grazing incidence technique was first proposed by the North-Western University group of Cohen et al.[11] It was developed and applied to the morphological characterization of nanoparticles on solid surfaces and of the nanostructures of thin films.[12,13]

In analyzing the GISAXS data, we consider sol−gel-derived vanadium and vanadium/cerium oxide films as aggregates containing nanosized grains and pores. Assuming that the SAXS signal is caused by the difference in electron density within and around the grain, their size distribution in the film can be determined.

Furthermore, two-dimensional (2-D) detection of the GISAXS signal gives an advantage of a more complex analysis, based on the comparison of the surface and bulk characteristics of the film. As well, a 2-D detector enables the probing of a wider reciprocal space range than a one-dimensional (1-D) detector. Since the experiment is done with grazing incidence, it is easier to separate the surface scattering contribution, which is concentrated mostly in the

* Corresponding author. Tel.:+385-21-385-633. Fax: +385-21-384-964. E-mail: malula@ktf-split.hr.
† University of Split.
‡ Institute Ruđer Bošković.
§ National Institute of Chemistry.

10.1021/ci050152j CCC: $30.25
Published on Web 10/25/2005

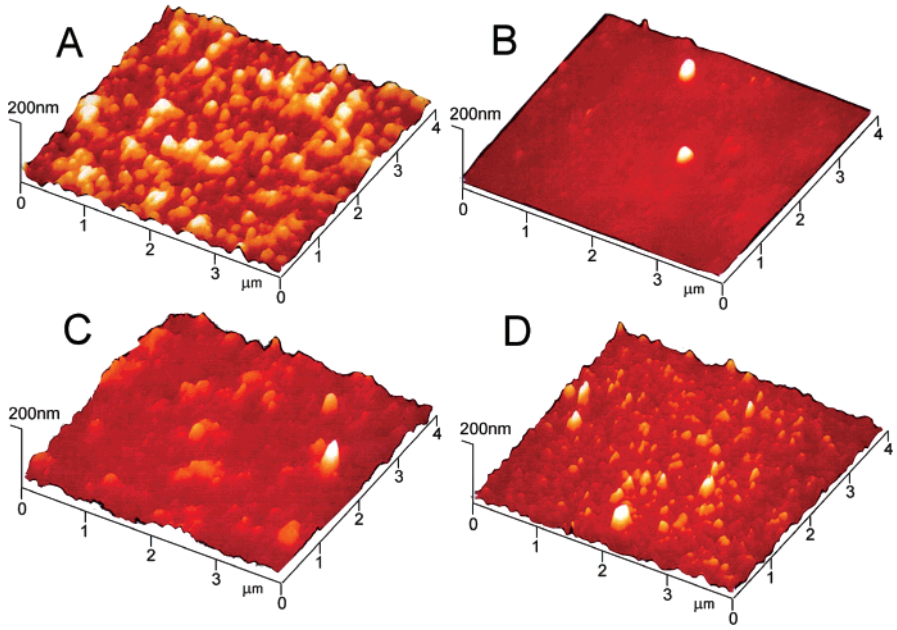

Figure 1. AFM micrographs for V oxide (sample A), nonintercalated V/Ce oxide with 38 atom % of V (sample B), Li-intercalated V oxide (sample C) and Li-intercalated V/Ce oxide with 38 atom % of V (sample D).

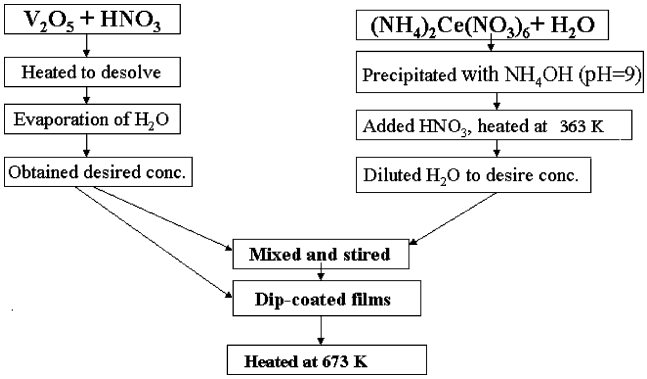

Figure 2. Schematic representation of the aqueous dip-coating sol−gel process for obtaining V oxides and V/Ce oxides.

specular plane, from the bulk contribution that is distributed more evenly over the detector area. The specular plane contains the incident wave vector and is perpendicular to the sample surface.

The investigation of V/Ce oxides with 2-D GISAXS has potential benefits for future work in the field of new nanostructured materials. Previously, these oxides were used as model samples for developing the grazing-incidence X-ray reflectivity (GIXR) method at the SAXS beamline,[5] and here their similar role regarding two-dimensional detection of scattering signal is presented.

2. EXPERIMENTAL SECTION

Vanadium oxide and mixed vanadium/cerium oxide films were obtained via the inorganic sol−gel process. Films were deposited by a dip-coating technique, following the scheme presented on Figure 2. Four samples were prepared: sample A, nonintercalated V oxide (V_2O_5); sample B, nonintercalated V/Ce oxide with 38 atom % of V; sample C, Li-intercalated V oxide; and sample D, Li-intercalated V/Ce oxide with 38 atom % of V. The conditions of sample preparation and intercalation of the lithium ions are described in previous publications.[10,14,15]

Scattering experiments were performed at the SAXS beamline,[16] at synchrotron ELETTRA in Trieste, Italy, using an X-ray beam energy of 8 keV (photon beam wavelength $\lambda = 0.154$ nm). The samples were examined in the form of layers deposited on glass substrates, using grazing incidence geometry. In this geometry, the incident angle of the X-rays with respect to the film surface is close to the critical angle of total external reflection. For incident angles larger than the critical, reflectivity decreases steeper than the value given by Fresnel theory because of deviations from ideal flatness.[17] When the incident angle is below the critical, the refracted beam is confined to the near surface layer.[18] With the change of incident angle, the penetration depth changes. In the case of our samples, the incident angle was on the order of 0.1°, well-above the critical angle, which was different for V and V/Ce oxides, to provide an adequate penetration depth of ~100 nm.

X-ray scattering intensity spectra were recorded by a fixed 2-D position-sensitive CCD camera (Photonic Science, type X-ray LA 1024/12, Roberts Bridge, U. K.), placed perpendicular to the horizontal incident X-ray beam. The samples were mounted on a stepper-motor-controlled tilting stage with a step resolution of 0.001° and aligned at a chosen grazing angle. The camera length of the setup was 2 m. For the angular (q-scale) calibration of the camera, the rat-tail tendon was used. The scattering wave vector $q = 4\pi \sin \theta/\lambda$, where 2θ is the scattering angle. On the recorded 2-D GISAXS intensity maps, like those in Figure 3, the scattering parallel and normal to the sample surface is distinguished, as indicated by respective components of the scattering vector, q_y and q_z. The maximum of the scattered intensity is in the direction of the so-called specular plane ($q_y = 0$), which is normal to the sample surface. This scattered intensity was partly reduced by a thin Al absorber.

The method of interpreting X-ray scattering data is based on the analysis of the scattering curve, which shows the dependence of the scattering intensity, I, on the scattering wave vector q. We extracted scattering curves from 2-D

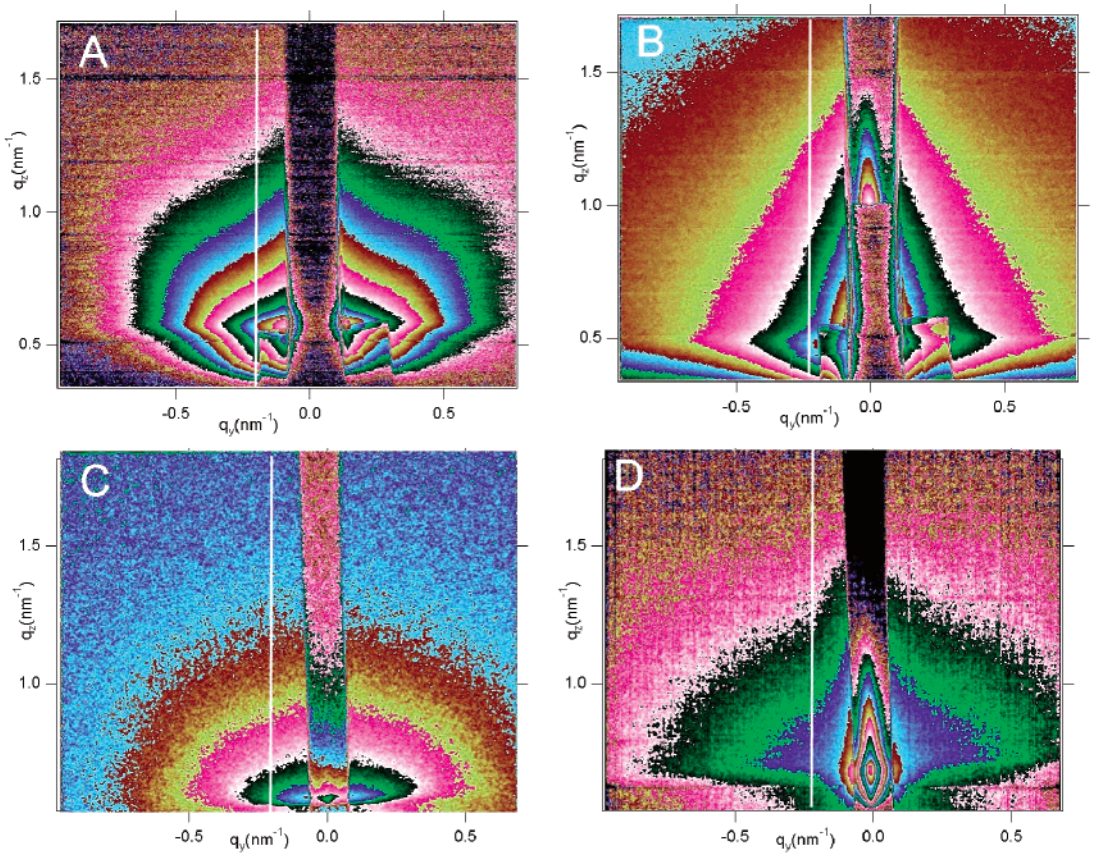

Figure 3. GISAXS patterns from V oxides (left, samples A and C) and V/Ce oxides (right, samples B and D), nonintercalated (top) and Li-intercalated (bottom).

GISAXS patterns of our samples as vertical scans (parallel to the specular plane) of scattered intensity versus the q_z component of the scattering wave vector. For further analysis of the scattering curves, self-made software was used. First, the measured intensities were corrected for absorption and refraction.[18] Then, the fitting of the experimental scattering curves was performed. In our previous investigations, we dealt with nanophased films of TiO_2, which were prepared by the similar sol−gel procedure. The grain size distributions were calculated on the basis of transmission electron microscopy and high-resolution electron microscopy studies of films, and the Gaussian fit was estimated as the best.[19] Therefore, in this case, we also used a simple model of spherical particles with a Gaussian size distribution. For the calculation of the scattering intensity, the following expression was used:

$$I(2\Theta) \equiv \int_{R_{MIN}}^{R_{MAX}} F(R,2\Theta) \exp[-(R - R_0)^2/\sigma^2]\, dR \quad (1)$$

in which the scattered intensity $I(2\Theta)$ is calculated as an integral of sphere form factor $F(R, 2\Theta)$ over a size range $[R_{MIN}, R_{MAX}]$ with maximum at R_0 and a half-width of half-maximum σ. This size range is wider than the experimental resolution, that is, minimum and maximum scattering angle, to account for the contribution from very small particles.

3. RESULTS AND DISCUSSION

Two-dimensional GISAXS intensity maps, that is, scattering patterns, for samples A, B, C, and D are shown in Figure 3. On the left and right are the scattering patterns from V and V/Ce oxides, respectively, while the top and bottom rows are nonintercalated and Li-intercalated scattering patterns, respectively. The maximum of the scattered intensity is in the direction of the specular reflection. The vertical strips in the patterns are the intensities depleted by the Al absorber, which was put in place to avoid detector saturation due to these high scattering intensities in the specular plane. The lower part of the scattering (below the surface plane) is missing from the pattern because of the absorption in the sample.

Besides this common feature, there are two types of contributions to scattering intensities, although of much lower intensities, that can be compared: diffuse scattering from the surface and particle scattering.

The diffuse scattering contribution from the surface is concentrated near the specular plane, and depending on the surface quality and roughness, it is the region where the scattering is usually orders of magnitude stronger than in other directions. In the case of a smooth surface with low roughness, it is also significant in a wider range around the specular plane, which can be seen in case of sample B, where the highest intensities are along the border of the absorber. In addition, when the scattering direction is at the critical angle with respect to the sample surface, the intensity is enhanced because of the refraction effects[18] ($q_z = 0.5$ nm^{-1} in the scattering pattern of sample B), and again, this is more pronounced for the surface contribution.

On the other hand, the particle scattering contribution is a function of the total scattering angle; that is, it is distributed symmetrically around the incoming beam direction regardless of the sample's orientation. Therefore, if well-defined and

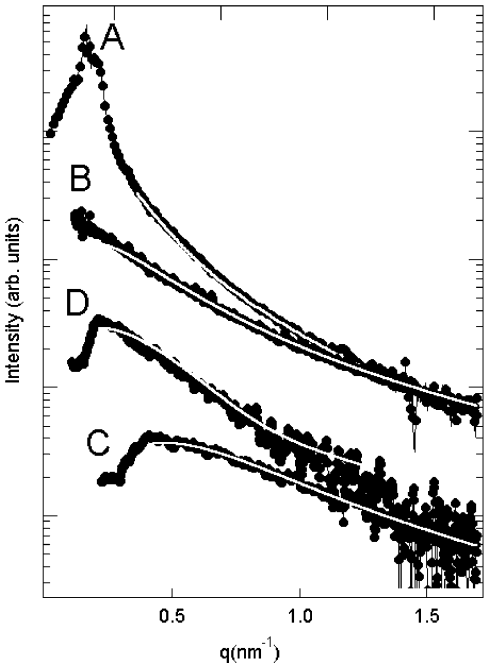

Figure 4. Fitting of the experimental scattering curve, I versus q, of samples A, B, C, and D to the calculated curve (I is intensity and scattering wave vector $q = 4\pi \sin \theta/\lambda$, where 2θ is the scattering angle and λ is the X-ray wavelength).

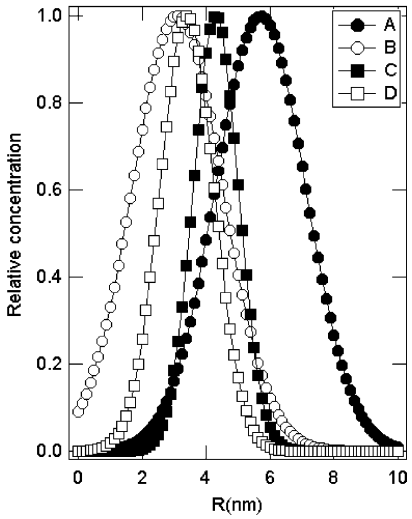

Figure 5. Size distributions of grains for samples A (—●—), B (—○—), C (—■—), and D (—□—). The mean grain sizes, R_m, and distribution half-widths, σ, are shown in Table 1.

randomly distributed particles are present in the film, they will cause additional diffuse scattering intensity far away from the specular plane. Since it is not incident-angle-dependent, this particle type of scattering can be easily separated from the surface scattering.

The presence of the particle type of scattering is a strong indication of the presence of the grains in the film. To assess the sizes of the grains, we have used the intensities parallel to, but away from, the specular plane (at $q_y = \sim 0.32$ nm^{-1}) to have minimal surface scattering influence. These are shown in Figure 4. The resulting size distributions of grains in the samples are shown in Figure 5. Errors are on the order of less than 0.1 nm.

Generally, V oxide samples show relatively stronger particle scattering than the respective V/Ce ones, as is indicated when comparing scattering from sample A with that from sample B. The cerium oxide structure tends to be more homogeneous; thus, there is a lower grain-to-grain border density contrast, resulting in a lower particle contribution intensity. In addition, because of homogeneity, the surface is smoother, thus, the stronger surface scattering. For V oxide, our particle scattering modeling determined the sizes to be centered at 5.7 nm with a half-width of 2.0 nm, while for V/Ce oxide, the sizes are centered at 2.1 nm with a half-width of 2.0 nm. Evidently, the model is not as good for the latter, since it gives a very wide relative size distribution. However, since very small particles had to be included in order to obtain a good fit, both a smooth structure and a smooth surface are supported by this model.

Table 1. The values of average grain size $\langle R \rangle$ (determined from 1-D GISAXS),[5] mean grain size R_m and distribution half-width σ (determined from 2-D GISAXS) and surface roughness χ (measured by AFM[10]) for V oxide and V/Ce oxide at 38 atom % of V, before (samples A and B) and after Li intercalation (samples C and D)

sample	GISAXS[5] $\langle R \rangle$ (nm)	R_m (nm)	σ (nm)	AFM[10] χ (nm)
A	5.39 ± 1.27	5.70 ± 0.22	2.0 ± 0.11	11
B	3.10 ± 0.58	2.10 ± 0.27	2.0 ± 0.11	2
C	3.43 ± 1.28	4.30 ± 0.12	1.0 ± 0.05	6
D	4.90 ± 0.43	3.40 ± 0.10	1.0 ± 0.04	8

The effects of the introduced Li are diverse for V and V/Ce oxides. While, in the case of V oxide, it resulted in both grain-size and distribution-width reductions (sizes centered at 4.3 nm, half-width of 1.0 nm), in the V/Ce oxide, mean grain size is increased to 3.4 nm but the distribution half-width is reduced to 1.0 nm. Generally, lithium introduction somehow reduces the difference in V and V/Ce structure preference for both grain size and distribution width, but it narrows the latter. Therefore, the surface contribution in V/Ce oxide is reduced, since its flatness is reduced by the presence of well-defined grains.

Although in a different size range, this is well-supported by the results of an AFM analysis,[10] as mentioned in the Introduction section. The values of root-mean square surface roughness, χ, estimated by AFM for V oxide and V/Ce oxides, prepared with two different concentrations of V via the route shown in Figure 2, are given in Table 1. For pure V oxide and V/Ce oxides with concentrations of V higher than 38 atom %, the value of χ is lowered after intercalation of lithium ions. To the contrary, in the case of V/Ce oxide with 38 atom % of V, the value of χ is exceptionally increased after the intercalation of lithium. Before intercalation, the surface of this particular V/Ce oxide (our sample C) appears to be smooth, with a χ value of 2 nm, in comparison to the surface of pure V oxide (our sample A), dominated by a grain-like structure and with a χ value of 11 nm. After intercalation, that is, in the cases of samples D and B, these values are changed to 8 and 6 nm for V/Ce and V oxide, respectively. Here, the V/Ce oxide surface is partly particle populated. The results of AFM measurements for samples A, B, C, and D are presented together with the results of the GISAXS analysis performed under 1-D and 2-D detection. Evidently, using GISAXS, we observed the same trend of structural modification that was observed by AFM. This justifies the application of the particle scattering model in our GISAXS data interpretation. It also shows that the surface quality is a consequence of the grained structure

and the surface roughness is a result of the sizes of the grains, which are similar on the surface and inside the film.

CONCLUSION

The present study shows that the application of the particle scattering model in analyzing the GISAXS measurements data can be utilized for estimating the structural properties of the vanadium/cerium oxide thin films as well as for following their structural modifications in the process of lithium intercalation. However, since SAXS analysis is model-dependent and suffers from the influence of various material properties, a two-dimensional detection of the scattering signal is applied and the results are compared to those of the AFM surface imaging. In conclusion, the observed aspects of the GISAXS intensity maps supported by the AFM analysis provide a contribution to the modeling of nanostructured intercalation electrodes.

ACKNOWLEDGMENT

The Ministry of Education, Science and Sport of the Republic of Croatia, under contract number 0098026, is thanked for its support of this work, as is the Ministry of Sciences and Technology of the Republic of Slovenia.

REFERENCES AND NOTES

(1) Lučić Lavčević, M.; Turković, A. *Thin Solid Films* **2002**, *419*, 105.
(2) Tonejc, A. M.; Turković, A.; Gotić, M.; Musić, S.; Vuković, M.; Trojko, R.; Tonejc, A. *Mater. Lett.* **1997**, *31*, 127.
(3) Turković, A.; Dubček, P.; Crnjak Orel, Z.; Bernstorff, S. *Nanostruct. Mater.* **1999**, *11*, 909.
(4) Turković, A.; Crnjak Orel, Z.; Kosec, M. *Sol. Energy Mater. Sol. Cells* **2000**, *62*, 392.
(5) Dubček, P.; Turković, A.; Crnjak Orel, Z.; Etlinger, B.; Bernstorff, S. *J. Chem. Inf.Comput. Sci.* **2004**, *44*, 290.
(6) Talledo, A.; Anderson, A. M.; Granquist, C. G. *J. Appl. Phys.* **1991**, *69*, 3261.
(7) Zhang, F.; Passerini, S.; Owens, B. B.; Smyrl, W. H. *Electrochem. Solid State Lett.* **2001**, *4*, A221.
(8) Veszelei, M.; Kullman, L.; Azens, A.; Granquist, C. *J. Appl. Phys.* **1997**, *81*, 2024.
(9) Crnjak Orel, Z. *Solid State Ionics* **1999**, *116*, 105.
(10) Crnjak Orel, Z.; Mušević, I. *Nanostruct. Mater.* **1999**, *12*, 399
(11) Levine, J. R.; Cohen, J. B.; Chung, Y. W.; Georgopoulos, P. *J. Appl. Cryst.* **1989**, *22*, 528.
(12) Thiaudiere, A.; Naudon, A. *J. Phys. IV* **1996**, *6*, 553.
(13) Kutsch, B.; Lyon, O.; Schmitt, M.; Menning, M.; Schmidt, H. *J. Appl. Cryst.* **1997**, *30*, 948.
(14) Crnjak Orel, Z.; Orel, B. *J. Mater. Sci.* **1995**, *30*, 2284.
(15) Crnjak Orel, Z.; Muševič, I.; Orel, B. *Nanoparticles in Solids and Solutions*; Fendler, J. H., Dekani, I., Eds.; Kluwer Academic Publishers: Norwell, MA, 1996; p 519.
(16) Amenitsch, H.; Bernstorf, S.; Laggner, P. *Rev. Sci. Instrum.* **1995**, *66*, 1624.
(17) Pynn, R. *Phys. Rev. B* **1992**, *45*, 602.
(18) Petrich, M. A.; Gleason, K. K.; Reimer, J. A. *Phys. Rev. B* **1987**, *36*, 9722.
(19) Tonejc, A. M.; Gotić, M.; Gržeta, B.; Musić, S.; Popovoć, S.; Trojko, R.; Turković, A.; Mušević, I. *Mater. Sci. Eng., B* **1996**, *40*, 177.

CI050152J